


## RESEARCH ARTICLE

# The anatomy and metabolome of the lymphatic system in the brain in health and disease

Wenbo He<sup>1,2,#</sup> ; You Jing<sup>1,3,#</sup>; Qianfen Wan<sup>4,#</sup>; Ke Xiao<sup>1,2</sup>; Kening Chen<sup>1,2</sup>; Yuan Lu<sup>1,2</sup>; Liang Li<sup>5</sup>; Yajie Tang<sup>1,2</sup>; Yunte Deng<sup>6,\*</sup>; Zhaohui Yao<sup>7,\*</sup>; Junqiu Yue<sup>6,\*</sup>; Gang Cao<sup>1,2,8,9,\*</sup>

<sup>1</sup> State Key Laboratory of Agricultural Microbiology, Huazhong Agricultural University, Wuhan, 430070, China.

<sup>2</sup> College of Veterinary Medicine, Huazhong Agricultural University, Wuhan, 430070, China.

<sup>3</sup> Department of Biomedical Engineering, University of North Texas, Denton, TX.

<sup>4</sup> Key Laboratory of Magnetic Resonance in Biological Systems, Wuhan Institute of Physics and Mathematics, Chinese Academy of Sciences, Wuhan, 430071, China.

<sup>5</sup> Department of Ophthalmology, Stanford University School of Medicine, Palo Alto, CA.

<sup>6</sup> Department of Pathology, Hubei Cancer Hospital, Wuhan, 430079, China.

<sup>7</sup> Department of Geriatrics, Renmin Hospital of Wuhan University, Jiefang Road, Wuhan, China.

<sup>8</sup> Bio-Medical Center, Huazhong Agricultural University, Wuhan, 430070, China.

<sup>9</sup> Cooperative Innovation Center for Sustainable Pig Production (CICSPP), Huazhong Agricultural University, Wuhan, 430070, China.

## Keywords

brain lymph fluid (BLF), glioma, metabolome, nuclear magnetic resonance (NMR), Parkinson's disease (PD).

## Corresponding author

Yunte Deng, Department of Pathology, Hubei Cancer Hospital, Wuhan 430079, China (Email: [tmdytok@163.com](mailto:tmdytok@163.com))

Zhaohui Yao, Department of Geriatrics, Renmin Hospital of Wuhan University, Jiefang Road, Wuhan, China (Email: [yaozhaohui2004@126.com](mailto:yaozhaohui2004@126.com))

Junqiu Yue, Department of Pathology, Hubei Cancer Hospital, Wuhan 430079, China (Email: [yuejunqiu@hotmail.com](mailto:yuejunqiu@hotmail.com))

Gang Cao, State Key Laboratory of Agricultural Microbiology, Huazhong Agricultural University, Wuhan 430070, China (Email: [gcao@mail.hzau.edu.cn](mailto:gcao@mail.hzau.edu.cn))

Received 25 June 2019

Accepted 10 November 2019

Published Online Article Accepted

20 November 2019

#These authors contributed equally to this work as first authors.

doi:10.1111/bpa.12805

## INTRODUCTION

The lymphatic system maintains immune surveillance (8, 11, 35) and tissue homeostasis via the recycling of interstitial fluid (ISF) (1, 28). For a long time, the brain was considered to lack a dedicated and conventional lymphatic system. Recently, emerging evidences have demonstrated that the brain has a lymphatic drainage system that is actively involved in parenchymal waste clearance, brain

## Abstract

Recent studies have demonstrated that the brain is equipped with a lymphatic drainage system that is actively involved in parenchymal waste clearance, brain homeostasis and immune regulation. However, the exact anatomic drainage routes of brain lymph fluid (BLF) remain elusive, hampering the physiological study and clinical application of this system. In this study, we systematically dissected the anatomy of the BLF pathways in a rat model. Moreover, we developed a protocol to collect BLF from the afferent lymphatic vessels of deep cervical lymph nodes (dcLNs) and cerebrospinal fluid (CSF) from the fourth ventricle. Nuclear magnetic resonance spectroscopy showed that BLF contains more metabolites than CSF, suggesting that BLF might be a more sensitive indicator of brain dynamics under physiological and pathological conditions. Finally, we identified several metabolites as potential diagnostic biomarkers for glioma, Parkinson's disease and CNS infectious diseases. Together, these data may provide insight into the physiology of the lymphatic system in the brain and into the clinical diagnosis of CNS disorders.

homeostasis and immune regulation (3, 37, 38). The lymphatic drainage system in the brain consists of a brain-wide glymphatic (glial-lymphatic) pathway, which includes the periarterial and perivenous spaces and glymphatic CSF-ISF flow in the brain parenchyma, and cerebrospinal fluid (CSF) drainage routes, which include dural-sinus-lined meningeal lymphatic vessels and olfactory/cervical lymphatic routes. In the glymphatic pathway, CSF flows into the brain along periarterial spaces and subsequently into the

brain interstitium, carrying metabolic products from ISF; then, CSF flows toward the perivascular spaces (22, 23, 46, 47, 58). In the CSF drainage routes, CSF is transported mainly to meningeal lymphatic vessels or to perineural spaces across the cribriform plate leading to the nasal mucosa (4, 13, 27, 29, 39, 41) and subsequently into cervical lymph nodes (3, 38, 42). These findings confirmed the presence of lymphatic vasculature in the brain, which serves as a draining route from brain ISF to peripheral lymph nodes. However, the exact anatomic drainage routes of brain lymph fluid (BLF) from cranial bone to peripheral lymph nodes need to be more precisely characterized.

The brain can produce different metabolic products under physiologic and pathological conditions, such as neurodegeneration, tumors and neuroinflammatory diseases initiated by neurotropic viruses or bacteria such as tubercle bacillus. These metabolic waste products need to be efficiently eliminated to maintain proper functioning in the brain. Some differentially produced metabolites have been considered diagnostic biomarkers (19, 54, 55). In most organs, venous return is a major drainage route for metabolic products. In the case of the brain, the blood–brain barrier (BBB), which separates circulating blood cells and solutes from the brain parenchyma and ISF (5, 16), makes venous blood in the brain only a component of micro-molecular metabolites. Thus, CSF, instead of venous blood in the brain, has been widely considered a major diagnostic target for brain diseases (7, 30, 33, 59). Owing to the great permeability of lymphatic vessels, it is reasonable to hypothesize that there are more brain metabolites in BLF than in CSF, and brain metabolites in BLF vary dynamically and may reflect more accurate physiological and pathological conditions of the brain. Therefore, monitoring the BLF of brain metabolites provides new insight into the clinical diagnosis of central nervous system (CNS) diseases.

The aim of this study is, therefore, to systematically dissect the brain lymph drainage routes to cervical lymph nodes and probe the potential novel diagnostic biomarkers from BLF for CNS diseases.

## MATERIALS AND METHODS

### Animals

Male Sprague Dawley rats (weighing over 220 g) were purchased from Hubei Disease Control and Prevention Center and were housed in temperature- and humidity-controlled rooms with a 12/12 h light/dark cycle (lights on at 7:00 am). All procedures were performed by following the regulations of the Institutional Animal Care and Use Committee of Huazhong Agricultural University (ethical review number: HZAURA-2015-007, approved by The Scientific Ethic Committee of Huazhong Agricultural University). Animals in the same experimental group were selected from different cages to assure randomization.

### Animal anesthesia

Compound anesthetic agents were used for anesthetizing animals. Briefly, 10% urethane and 2% chloral hydrate were mixed with 3 mg/mL xylazine (Sigma-Aldrich, USA) at a ratio of 3:1, diluted with ddH<sub>2</sub>O and stored at 4°C in the short term or –20°C in the long term. For a short operation period (less than 5 min), isoflurane was used instead of compound anesthesia.

### Evans blue injection

Rats were anesthetized with the compound anesthetic agent (0.9 mL/100 g, i.p.), and then 10 or 20 µL of 10% Evans blue (Sigma-Aldrich, USA) was injected into the left lateral ventricle (AP: –0.95, ML: –1.9, DV: 3.8) using a stereotaxic apparatus (RWD, China). Thirty minutes after injection, facial and cervical skin were removed.

### BLF sample collection

For BLF sample collection, cervical skin was incised, and muscles were separated bluntly to expose deep cervical lymph nodes. In conjunction with the circulation of Evans blue, brain-related lymphatic vessels were dyed to distinguish them from other vessels. The afferent vessels of the dcLNs were selected for the BLF sample collection. With the help of a needle hook, a single lymphatic vessel was isolated and cut to collect 30–100 µL of BLF. A 100 µL microsyringe (Gaoe, China) was used to collect the BLF.

### CSF sample collection

The CSF was collected by making a skin incision between the ears, and blunt dissection was performed at the base of the cranial muscles to expose the foramen magnum. Stroke-physiological saline solution (0.9% NaCl) was used to wash blood away from the foramen magnum. A 1 mL microsyringe was used to penetrate the fourth cerebral ventricle through the foramen magnum at an angle of 20–30 degrees in the horizontal plane for collection of 100 µL of CSF.

### Glioma animal model

Rats were anesthetized with compound anesthetic agent (0.9 mL/100 g, i.p.) and mounted on a stereotaxic frame. A total of 10<sup>4</sup> C6 glioma strain cells (Hualianke Company, China) were injected into the right striatum at three sites (AP: 0.95, ML: 2.6, DV: 3.5), (AP: 0.95, ML: 2.6, DV: 4.0) and (AP: 0.95, ML: 2.6, DV: 4.5) through a 10 µL microsyringe (Gaoe, China) at a rate of 0.5 µL/min. Then, the same amount of PBS was injected into the counterpart regions of control rats. After the infusion, the microsyringe was left at the target site for an additional 10 min to allow diffusion. At 21 days postoperation, careful attention was paid to monitoring the pathological status of the rats, and weights were documented each

day. When the rats appeared weak and their weight dropped significantly (over 10 g per day), BLF was collected immediately. After collection, the rats were perfused with PBS and 4% PFA. Then, the brains were extracted and fixed in 4% PFA overnight. The success of glioma model construction was further confirmed by the appearance of glioma tissue in the striatum by brain paraffin sectioning and H&E staining.

### Virus infection model

Rats were anesthetized by isoflurane inhalation (RWD, China). A GFP-expressing pseudorabies virus 152 (PRV152) was injected intramuscularly into the forelimbs, with 10  $\mu$ L (virus titer 10E8) injections on each side. Then, the same amount of PBS was injected into the counterpart region of control rats. At 120 h postinjection, the rats were anesthetized with a compound anesthetic agent (0.9 mL/100 g, i.p.) for BLF collection. Then, rats were perfused with PBS and 4% PFA. Brains were extracted and fixed in 4% PFA.

### Parkinson's disease animal model

Following anesthetization of rats with the compound anesthetic agent (0.9 mL/100 g, i.p.), 6-OHDA was used to construct the PD model via intracerebral injection at three sites (AP: 0.95, ML: 2.6, DV: 3.5), (AP: 0.95, ML: 2.6, DV: 4.0) and (AP: 0.95, ML: 2.6, DV: 4.5) into the right striatum. A total of 10  $\mu$ L 6-OHDA (1  $\mu$ g/ $\mu$ L; Sigma, USA) in 0.9% NaCl solution with 0.02% ascorbic acid was used for infusion into the brain via a 10  $\mu$ L microsyringe at a rate of 0.5  $\mu$ L/min. The same amount of PBS was injected into the counterpart regions of control rats. After infusion, we left the microsyringe at the target site for an additional 10 min to allow diffusion. Three weeks after the injection, the effectiveness was assessed using the test of contralateral rotational behavior induced by apomorphine (0.5 mg/kg; i.m.) dissolved in 0.9% NaCl solution at a concentration of 1 mg/mL. The lesion was considered successful if the rat made over 210 rotations per 30 min in the contralateral direction. The rats with successful lesions were used for lymphatic fluid collection. After collection, the rats were perfused with PBS and 4% PFA, and the brains were extracted for fixation in 4% PFA.

### Sample preparation for NMR and $^1\text{H}$ NMR spectroscopy

BLF and CSF samples (approximately 30  $\mu$ L) were separately mixed with 30  $\mu$ L of phosphate buffer solution for NMR analysis. The phosphate buffer (45  $\mu$ M) prepared by dissolving  $\text{K}_2\text{HPO}_4/\text{NaH}_2\text{PO}_4$  4:1 into 0.9% NaCl deuterated water ( $\text{D}_2\text{O}$ ) was used to lock the frequency of the spectrometer during sample acquisition. All the NMR experiments were conducted on a Bruker Avance III 600 MHz NMR spectrometer equipped with an inverse detection cryoprobe (Bruker Biospin, einstein, Germany) at 298 K. The Carr–Purcell–Meiboom–Gill pulse program ((RD–90°–( $\tau$ –180°– $\tau$ )n-acquisition);  $\tau$  = 350  $\mu$ s, n = 100)

with water suppression pulse sequences was used to suppress NMR signals from macromolecules with a shorter  $T_2$  relaxation time and to retain signals from low-molecular weight metabolites with longer  $T_2$  relaxation times. Each BLF and CSF spectrum with a spectral width of 20 ppm contained 128 scans, and each scan consisted of 32 k data points. For the purpose of signal assignments, a set of two-dimensional NMR spectra,  $^1\text{H}$ – $^1\text{H}$  correlation spectroscopy (COSY),  $^1\text{H}$ – $^1\text{H}$  total correlation spectroscopy (TCOSY),  $^1\text{H}$  J-resolved,  $^1\text{H}$ – $^{13}\text{C}$  heteronuclear single quantum correlation (HSQC) and  $^1\text{H}$ – $^{13}\text{C}$  multiple bond correlation spectra (HMBC), were recorded as described in a previous study (14, 15, 57).

### NMR spectrum processing and statistical analysis

The processing of all NMR spectra was conducted with Topspin software. Zero-filled to 128 k points and exponential window functions with 1 Hz line-broadening were applied to all spectra prior to Fourier transformation, followed by manual phase and baseline adjustments. The spectral regions of 0.8–8.8 ppm were integrated into bins of 0.002 ppm with Amix software. The processed data were further exposed to Multiple Univariate Data Analysis (MUDA) using MATLAB script. A previous study described the detailed MUDA analysis (18). In short, the MUDA analysis was based on either Student's *t*-test or nonparametric tests. The difference in metabolite concentrations in the groups is presented in a differential metabolome plot, in which statistically significant metabolites ( $P < 0.05$ ) are colored red.

### Sample preparation and H&E staining

All rat brains were fixed in 4% PFA, following the standard principles for dehydration, waxing, and embedding of brain samples. The tissue sections were prepared with an Ultra-Thin Semiautomatic Microtome (Leica, Germany) or a freezing microtome (Leica, Germany). Brain slices were 4  $\mu$ m thick for paraffin sections and 20  $\mu$ m thick for frozen sections. To verify the construction of each model, H&E staining was performed.

### Immunohistochemistry and immunofluorescence

Sections were baked in a 37°C dryer for 12 h and in a 60°C dryer for 1 h. Sections were then deparaffinized in xylene and rehydrated in descending dilutions of ethanol. For paraffin-embedded sections, we performed antigen retrieval procedures in the microwave, with circulation for 2 min under moderate heat and 8 min at room temperature for a total of 3 times. Slices were washed with PBS and blocked with 2% BSA at room temperature for 1 h. Anti-tyrosine hydroxylase (TH) (ab6211) antibody was used to confirm the decrease in TH-positive neurons in the right striatum. Briefly, 1:400 diluted primary antibody was added to the slices and incubated overnight at 4°C. Biotinylated

anti-rabbit IgG was used as a secondary antibody, and DAB substrate was used for staining these sections. Anti-LYVE1 primary antibody (Abcam, USA) was used to confirm the lymphatic vessel characteristics of cervical LN-related ducts. Then, 1:400 diluted anti-LYVE1 was added to the ducts and incubated overnight at 4°C. A 1:300 diluted secondary antibody (Alexa Fluor 488, Thermo Fisher Scientific, USA) was then incubated for 2 h at room temperature. After secondary antibody washing, tissue sections were mounted with 50% glycerol. Immunofluorescence images were taken by fluorescence microscopy (Olympus, Japan).

## RESULTS

### Dissection of the BLF drainage anatomic routes from the cranium to dcLNs and scLNs

To systemically delineate the BLF drainage anatomic routes from the cranium to cervical lymph nodes, different amounts of Evans blue were injected into the lateral ventricle to optimize the visualization of BLF drainage (Figure 1A) ( $n = 3$ ). We found that waiting 30 min after injection of 10  $\mu\text{L}$  Evans blue was enough time to visualize the bilateral deep cervical lymph nodes (dcLNs) and related vessels (Figure 1B) ( $n = 5$ ). For superficial cervical lymph nodes (scLNs), the optimal injection condition was 20  $\mu\text{L}$  Evans blue, as the scLNs remained gray or slightly blue with an injection of 10  $\mu\text{L}$  Evans blue (Figure 1C) ( $n = 5$ ). Figure 1B,D shows that dcLN- and scLN-related BLF vessels obviously extended into separate pathways. dcLN-related interlacing afferent ducts arose near the internal jugular vein, stretched along the trachea in the neck and medial pterygoid bone in the base of the skull, and eventually exited via foramina at the base of the skull (Figure 1B). scLN-related afferent ducts extended along the masseter muscle under the facial and cervical skin. A portion of scLN ducts crossed through the infra-orbital foramen, while the others exited via the nasal cavities. Finally, both ducts traveled in a retrograde fashion to the cribriform plate at the front of the base of the skull (Figure 1E). The integrated BLF drainage routes from the cranium to dcLNs and scLNs are illustrated in Figure 1F.

The lymphatic characteristics of dcLN- and scLN-related afferent vessels were further examined by assessing the presence of the classic lymphatic vessel marker, lymphatic vessel endothelial hyaluronan receptor 1 (LYVE-1). Immunofluorescence staining of the vessels showed that LYVE-1-positive lymphatic vessels drained BLF from the cranium to cervical lymph nodes (Figure 1G). Moreover, we developed a protocol to collect original BLF before dcLNs to avoid the degradation of brain metabolites in lymph nodes, as shown in Figure 1H. By taking advantage of this strategy, we collected, to our knowledge, the first BLF sample from dcLNs. The BLF with Evans blue dye could be collected from the afferent vessels of the dcLNs (Figure 1H) and scLNs (Figure 1I). These data further support that the identified vessels are indeed BLF drainage routes.

It is conceivable that pathological brain conditions (such as glioma) could influence the pathophysiological condition

of dcLNs and scLNs, as the first lymph nodes of BLF drainage. To test this hypothesis, we established a rat glioma animal model by injecting C6 glioma cells in the rat striatum and investigated the morphology of dcLNs and scLNs. Both dcLNs and scLNs connected to brain lymphatic vessels appeared to have pathological changes (Figure 1J), such as an expansion of the subcapsular sinus, an increasing number of macrophages and lymphocytes, as well as a decreasing number of desmocytes, in the subcapsular sinus. Similar LNs pathological changes were observed under virus infection and PD conditions. For LNs in PD model, the expansion of the subcapsular sinus were smaller than that of the glioma and virus models, probably due to PD progressed slowly and caused less inflammation in LNs. These data further indicate that BLF can drain towards dcLNs and scLNs. Notably, we observed that the dcLN pathway might be the first relay of BLF, as dcLNs became blue prior to scLNs, although both are associated with the lymphatic drainage system in the brain and are active in response to brain disorders.

### Comparison of Metabolites in BLF and CSF

As dcLNs were demonstrated as the first relay of BLF, we collected 30  $\mu\text{L}$  or more BLF from the afferent vessels of the dcLNs ( $n = 8$ ), as well as the same volume of CSF from the fourth ventricle ( $n = 9$ ), and these samples were subsequently subjected to NMR analysis. A total of 31 metabolites were identified from the NMR spectra in BLF (Figure 2A, Table S1), and these metabolites were further validated by various 2D NMR spectra. The spectra of the BLF contained signals from glucose, organic acids (eg, lactate, acetoacetate and N,N-dimethylglycine), amino acids (eg, alanine, leucine, valine, isoleucine, lysine, tyrosine, glycine, histidine, methionine and phenylalanine), glycoprotein (eg, O-acetyl glycoprotein and N-acetyl glycoprotein) and tricarboxylic acid (TCA) intermediates (citrate and succinate). Out of 31 metabolites, only 21 metabolites were detected in CSF (Figure 2B). Student's *t*-test was used to evaluate the significance of difference in metabolites between CSF ( $n = 9$ ) and BLF ( $n = 8$ ). Twenty out of 21 metabolites in BLF had a significantly higher concentration than in CSF ( $P < 0.01$ ) (Figure 2C). These NMR results showed that more metabolites could be detected in BLF than in CSF, suggesting that BLF was enriched with more metabolites and may more accurately reflect the pathophysiological status of the brain.

### BLF metabolome fluctuation under glioma conditions

Glioma is the most common malignant tumor of the central nervous system. To investigate the BLF metabolome of the brain in glioma, the rat brain glioma tumor model was established by injecting C6 cells into the right striatum ( $n = 8$ ). As shown in Figure 3A,B, there were a number of glioma cells and lymphatic cells in the section of striatum of the brain, as shown by H&E staining. Next, we collected 30  $\mu\text{L}$  BLF from the ipsilateral afferent lymphatic



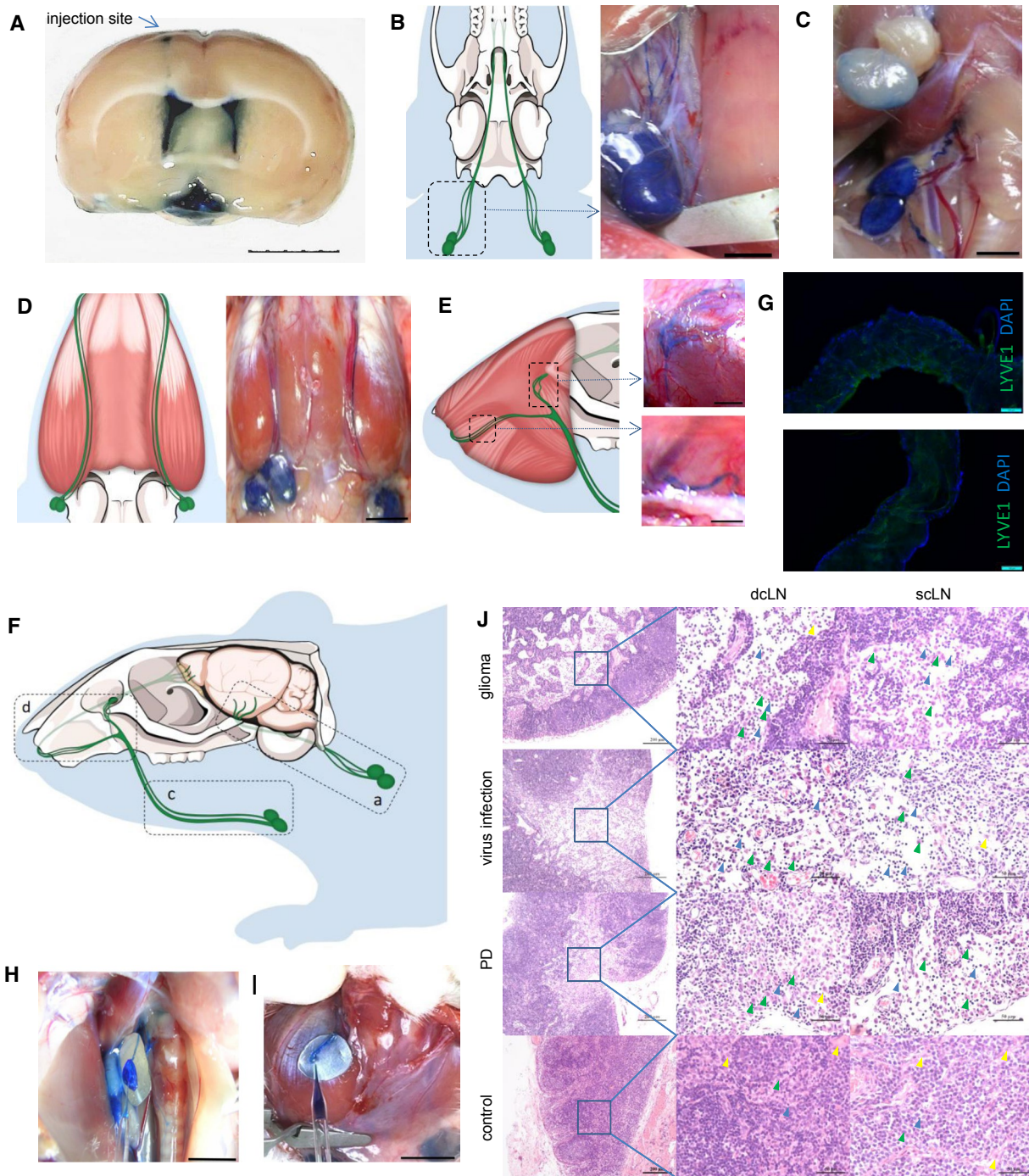


**Figure 1.** Anatomical structures of rat BLF drainage routes to cervical lymph nodes. **A**, Evans blue was injected into the lateral ventricle to optimize the visualization of BLF drainage. (n = 3) Bar: 5 mm. **B**, 30 min after, 10  $\mu$ L of 10% Evans blue was injected into the lateral ventricle, dcLNs and their afferent vessels were dyed blue, whereas scLNs and their vessels remained gray or slightly blue. **C**, (n = 5) Bars: 2 mm. **D**, 30 min after injection of 20  $\mu$ L Evans blue, scLNs and their afferent vessels became dark blue after dcLNs. (n = 5) Bar: 5 mm. **E**, A portion of scLN afferent vessels crossed through the infraorbital foramen, while the others exited via the nasal cavities. Bars: 2 mm. **F**, Schematic diagram of rat BLF drainage routes from the cranium to cervical lymph

nodes. **G**, Immunofluorescence of dcLN- and scLN-related afferent vessels for LYVE-1. Bars: 100  $\mu$ m. **H**, Collection of BLF from dcLN afferent vessels. Bar: 5 mm. **I**, Collection of BLF from scLN afferent vessels. Bar: 5 mm. **J**, Both dcLNs and scLNs connected to brain lymphatic vessels appeared to have pathological changes in brain glioma, virus infection and PD models, including the expansion of the subcapsular sinus, increasing of macrophages and lymphocytes, decreasing of desmocytes in the subcapsular sinus. Green arrowheads: macrophages, blue arrowheads: lymphocytes, yellow arrowheads: desmocytes. Bars: 200  $\mu$ m and 50  $\mu$ m.

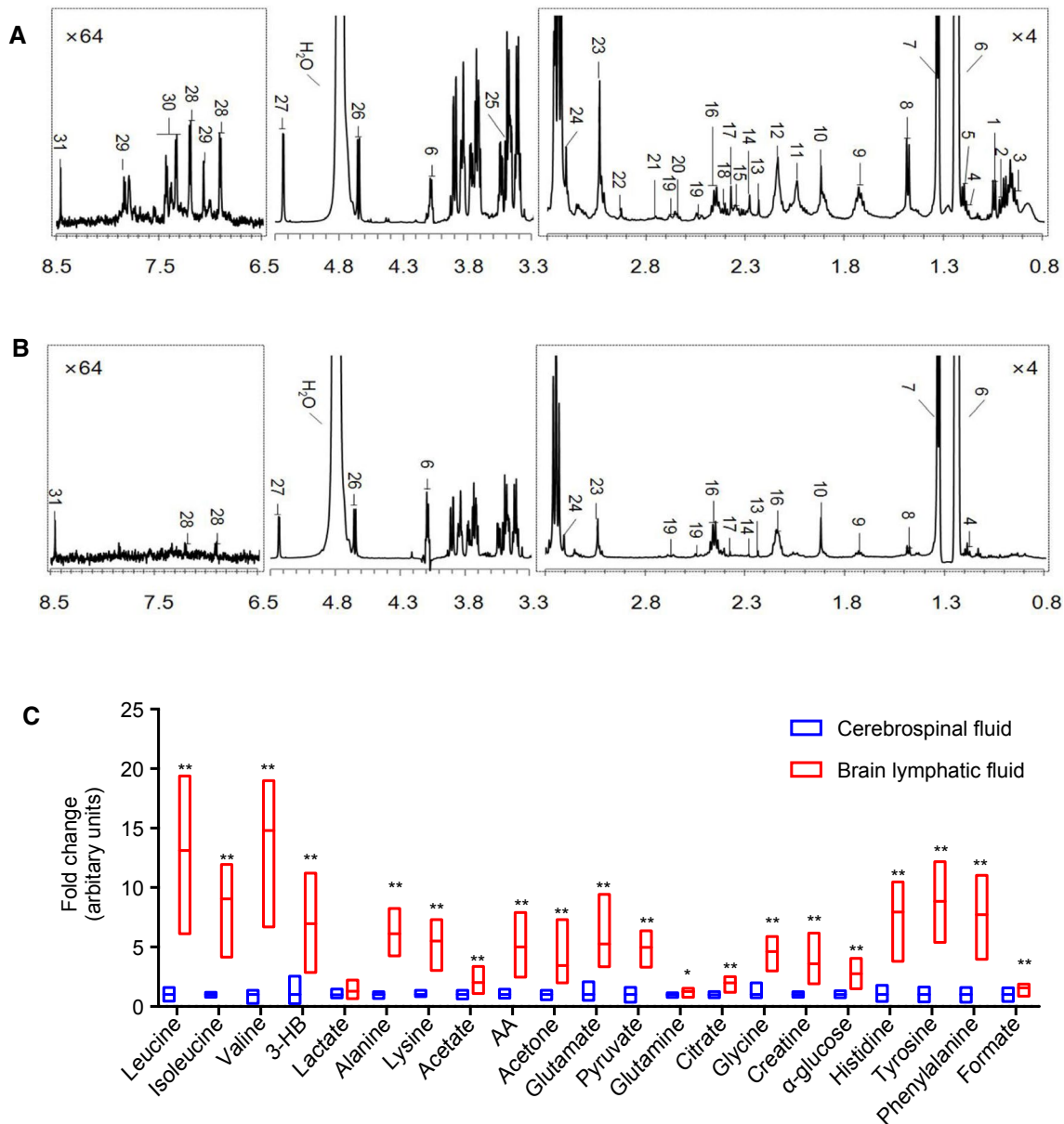


**Figure 2.**  $^1\text{H}$  NMR spectra of BLF and CSF from healthy rats, and concentrations of metabolites in BLF and CSF. **A**, The spectrum of BLF. The spectral regions of  $\delta$  0.8–3.3 and  $\delta$  6.5–8.5 were amplified 4 and 64 times, respectively, compared with the region of  $\delta$  3.3–5.3. A total of 31 metabolites were identified from the NMR spectra in BLF. ( $n = 8$ ). **B**, The spectrum of CSF. A total of 21 metabolites were detected in CSF.

Metabolite keys are listed in Table S1. ( $n = 9$ ). **C**, The relative concentration difference in metabolites between BLF and CSF from healthy rats, suggesting that BLF was enriched with more metabolites. Student's  $t$ -test was used to evaluate the significance of difference in metabolites between CSF ( $n = 9$ ) and BLF ( $n = 8$ ). \* $P < 0.05$ , \*\* $P < 0.01$ .

vessels of dcLNs and subjected the samples to NMR. Multiple univariate data analysis (MUDA) and Student's  $t$ -test were used to evaluate the significance of difference in metabolite concentrations between control rats ( $n = 8$ ) and glioma rats ( $n = 8$ ). Figure 3C,D demonstrated that the concentrations of ten metabolites (lactate, pyruvate, 3-hydroxybutyrate (3-HB), N-acetyl-glycoprotein (N-AG), O-acetyl-glycoprotein (O-AG), acetone, acetoacetate (AA),

creatine,  $\alpha$ -glucose and phenylalanine) were significantly different between glioma BLF samples and control samples. As shown in Figure 2C, among the 10 metabolites, 2 metabolites (N-AG and O-AG) could be detected in BLF but not in CSF. Among the remaining eight metabolites, seven metabolites (pyruvate, 3-HB, acetone, AA, creatine,  $\alpha$ -glucose, phenylalanine) had significantly lower relative concentrations in CSF than in BLF. These ten metabolites

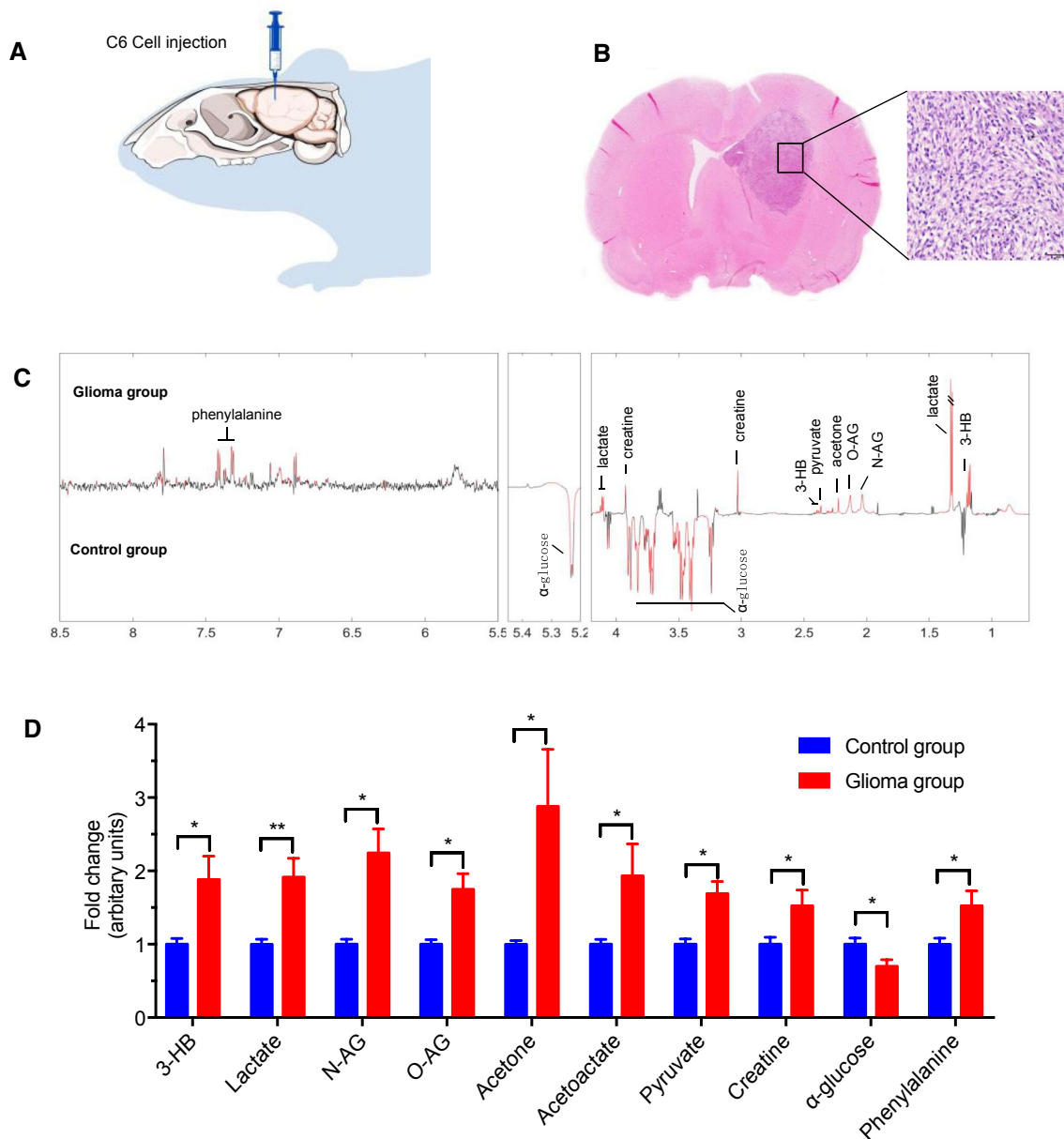


**Figure 3.** Brain morphologic changes and BLF metabolome fluctuations under glioma conditions. **A**, Injection of C6 glioma cells in the right striatum. (n = 8). **B**, Twenty-two days after the injection, glioma tissue was found in the striatum with a number of glioma cells and lymphatic cells. Bar: 50 μm. **C**, Differential-metabograms of BLF from control rats (n = 8) and glioma rats (n = 8). Metabolites with red color are significantly changed between groups. Multiple univariate data analysis (MUDA) was used to evaluate the significance of difference in metabolite

concentrations between groups. **D**, Relative concentrations of ten metabolites (3-hydroxybutyrate (3-HB), lactate, N-acetyl-glycoprotein (N-AG), O-acetyl-glycoprotein (O-AG), acetone, acetoacetate (AA), pyruvate, creatine, α-glucose, and phenylalanine) showing significant differences between glioma BLF samples and control samples. Student's t-test was used to evaluate the significance of difference in metabolites between two groups of samples. \*P < 0.05, \*\*P < 0.01.

might potentially be used as biomarkers for glioma diagnosis in the future.

**BLF metabolic disturbances with viral infection**

Next, we aimed to investigate the BLF metabolome during neurotropic viral infection. To this end, a neurotropic virus,

the pseudorabies virus expressing GFP, PRV152, was injected into rat forelimbs as a neurotropic virus infection model (53) (n = 9). As shown in Figure 4A,B, the GFP fluorescence signal in hippocampus and cerebral cortex M1 zone neurons validated the successful infection of PRV152. Then, 30 μL of BLF was collected from the ipsilateral afferent lymphatic vessels of dLNs and subjected to NMR



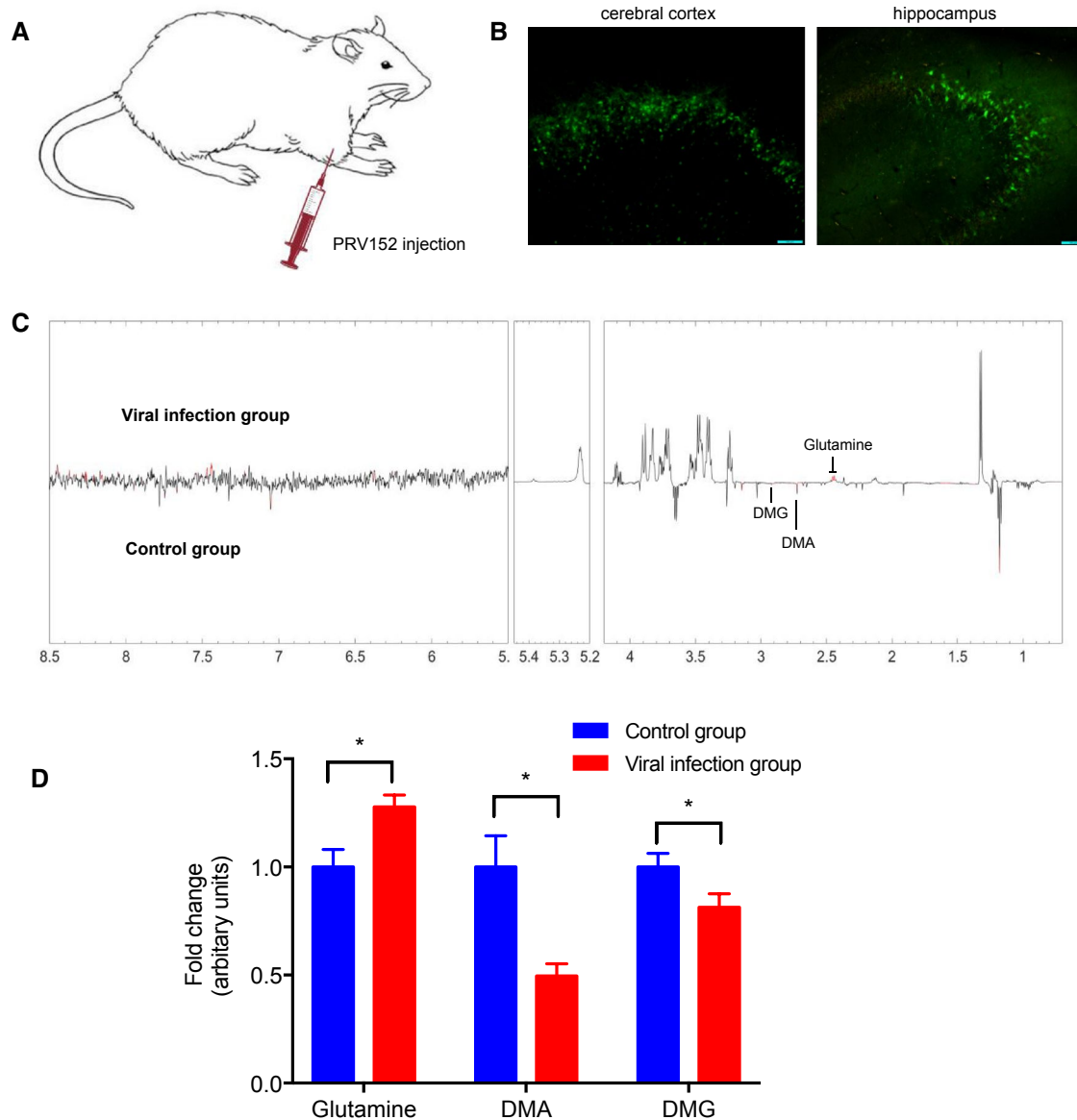


**Figure 4.** BLF metabolic disturbances with viral infection. **A**, Virus infection models. A neurotropic virus, the pseudorabies virus expressing GFP, PRV152, was injected into rat forelimbs as a brain viral infection model. ( $n = 9$ ). **B**, Four days after infection, infected neurons were observed in the hippocampus and cerebral cortex M1 zone. Bars: 100  $\mu\text{m}$ . **C**, Differential-metabograms of BLF from control rats ( $n = 10$ ) and viral infection rats ( $n = 9$ ). Metabolites with red color are significantly changed between groups. MUDA were used to evaluate the significance

analysis. Then MUDA and Student's *t*-test were used to evaluate the significance of difference in metabolite concentrations between control rats ( $n = 10$ ) and viral infection rats ( $n = 9$ ). The NMR data demonstrated that two metabolic disturbances (dimethylamine (DMA), N,N-dimethylglycine (DMG)) were significantly ( $P < 0.05$ ) lower and Glutamine was significantly higher ( $P < 0.05$ ) in the BLF of the viral infection group than in the BLF of the control group (Figure 4C,D). According to Figure 2C,

of difference in metabolite concentrations between groups. **D**, In the BLF of the viral infection group, dimethylamine (DMA) and N,N-dimethylglycine (DMG) were significantly lower, while glutamine was significantly higher than that of the control group. Student's *t*-test was used to evaluate the significance of difference in metabolites between control rats and viral infection rats.  $*P < 0.05$ .

two metabolites (DMA and DMG) were detected in BLF but not in CSF. While glutamine was also found in CSF, it was significantly lower ( $P < 0.01$ ) than in BLF.

#### BLF metabolome in Parkinson's disease (PD) models

To establish a PD model, 6-hydroxydopamine (6-OHDA) was injected into the right striatum (Figure 5A) ( $n = 7$ ).



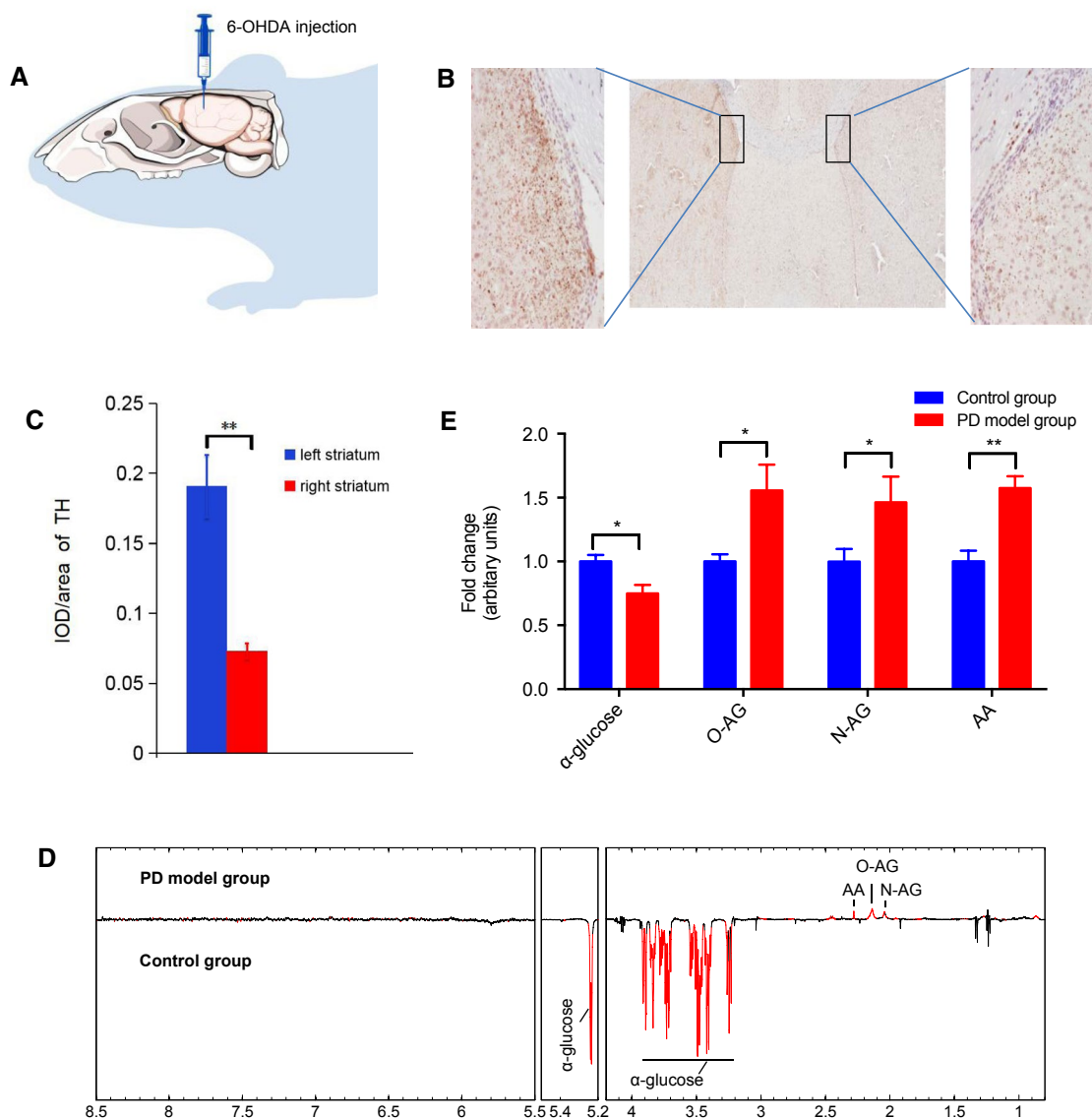


**Figure 5.** The BLF metabolome under the condition of Parkinson's disease. A, Brain infection with 6-hydroxydopamine (6-OHDA) to selectively destroy dopaminergic and noradrenergic neurons in the right striatum. (n = 7). B,C, 21 days after the infection, TH-positive neurons decreased sharply in the right striatum compared to the left striatum. Bars: 200  $\mu$ m. D, Differential-metabograms of BLF from control rats (n = 8) and 6-OHDA injection rats (n = 7). Metabolites with red color are significantly changed between groups. MUDA were used to evaluate

the significance of difference in metabolite concentrations between groups. E, Relative change fold of significant metabolites (acetoacetate (AA), N-acetylglycoprotein (N-AG), O-acetyl-glycoprotein (O-AG) and  $\alpha$ -glucose). Student's t-test was used to evaluate the significance of difference in metabolites between between the PD group and control group. \* $P < 0.05$ , \*\* $P < 0.01$ .

The PD model was validated by the assay of contralateral rotational behavior induced by apomorphine, and it resulted in sharply decreased tyrosine hydroxylase (TH)-positive neurons in the striatum 3 weeks after injection (Figure 5B,C). BLF was collected only from rats with a successful behavior assay. NMR, MUDA and Student's *t*-test analysis showed that four brain metabolites (N-AG, O-AG, AA and  $\alpha$ -glucose) were significantly different between the PD model (n = 7) and control groups (n = 8) (Figure 5D). According to Figure 2C, N-AG and O-AG were detected

in BLF but not in CSF. While  $\alpha$ -glucose and AA could also be detected in CSF, their concentrations were significantly lower ( $P < 0.01$ ) than those in BLF. These four metabolites might potentially be used as biomarkers for PD diagnosis in the future.

## DISCUSSION

The extracellular fluid of the brain consists of CSF, which exists in the ventricles, subarachnoid space and ISF in the

extracellular spaces of the brain parenchyma. While recent studies have established the concept that the glymphatic system carries brain metabolic products from ISF to CSF, it still remains elusive how exactly the CSF eliminates brain waste products. An obvious way that this elimination occurs is via dural sinuses, through which brain waste products are transported to the bloodstream. Another important elimination route is via brain lymphatic vessels that are located in the dura mater, which lines the dural sinuses (31, 38), or along the cranial nerves (2). Recently, experimental evidence has suggested that meningeal lymphatic vessels can even invade the brain parenchyma to guide vascular regeneration under cerebrovascular injury conditions (12). Therefore, brain lymphatic vessels play an important role in collecting brain metabolites, draining waste products into nearby lymph nodes (38) and helping the brain maintain homeostasis. Moreover, it has been demonstrated that brain lymphatic clearance dysfunction could participate in the pathogenesis of neurodegenerative diseases (10, 60). In line with this, we demonstrated that the BLF metabolomes from a PD model group and a control group were indeed different.

While recent evidence has demonstrated that the brain has a lymphatic drainage system for parenchymal waste clearance, brain homeostasis and immune regulation (3, 37, 38), the detailed anatomy of this pathway has not been systematically investigated. Previous studies showed that CSF was drained from the subarachnoid space to dCLNs but not to sCLNs (3) by injecting 5  $\mu$ L Evans blue *i.c.v.* into mice and PEG-IRDye into the brain parenchyma of Prox1-GFP mice. In our study, we demonstrated that both the bilateral dCLNs and sCLNs were labeled with Evans blue dye 30 min after injection with 20  $\mu$ L of Evans blue into the rat brain. This discrepancy could be due to the injection amount of the dyes. Anatomical findings and histological results have revealed that the inferior nasal turbinate contains numerous lymphatic tissues and is connected to the nasolacrimal duct ensheathed by a dense network of lymphatics (36). Furthermore, there is ample evidence suggesting that CSF drains via the cribriform plate into the nasal mucosa (24, 32, 56). Together, these results suggest the existence of lymphatic outflow routes of CSF (namely, BLF) in the nasal cavity. Notably, we showed that intranasal BLF subsequently drained into sCLNs.

Our study systematically delineated the pathways of BLF drainage and demonstrated that this sophisticated lymphatic vasculature mainly comprised two main routes: (i) dural lymphatic vessels that flow from the dura mater via foramina at the base of the skull into dCLNs; and (ii) channels lining the olfactory nerves that deliver fluid into the nasal mucosa and then to sCLNs. Our findings characterized the final step in BLF drainage of ISF from the brain parenchyma into peripheral LNs. We speculated that BLF was preferentially drained via the dCLN route, as the dCLN pathway became blue prior to sCLN pathway after *i.c.v.* injection. sCLN route might carry out a small amount of BLF as a supplementary pathway of BLF drainage under elevated intracranial pressure. The drainage of CSF is not

only significant for volume regulation but also for the clearance of brain metabolic waste products. Accumulating studies have demonstrated that CSF dynamics can reflect many pathological conditions of the brain and are clinically applied for the diagnosis of many diseases, including hydrocephalus (17, 34), intracerebral hemorrhage (21, 51), idiopathic intracranial hypertension (45, 50), large hemispheric stroke (6, 40), subarachnoid hemorrhage (9, 43), traumatic brain injury (25, 26) and brain aging (49, 52). In fact, soluble amyloid beta-protein ( $A\beta$ ) and apolipoprotein E levels in CSF are significantly lower in patients with definite Alzheimer's disease (AD) (20, 44). Moreover, it has been shown that there is a substantial decrease in the levels of total secreted  $\beta$ -amyloid precursor protein (sAPP), sAPP-alpha (sAPP $\alpha$ ) and  $A\beta$ (1–19, 21–43) in the CSF of normal pressure hydrocephalus (NPH) patients who may develop AD-like pathology (48). However, CSF contains only a small portion of the metabolites in the brain and thus is a great limitation to accurately reflecting the pathophysiological status of the brain.

Due to the great permeability of lymphatic vessels, BLF may accumulate more kinds of brain metabolites than CSF. Thus, BLF might have a better capacity than CSF to accurately reflect the pathophysiological status of the brain. In the current study, we developed a protocol to collect BLF from the afferent vessels of dCLNs and compared brain metabolites between BLF and CSF by NMR. Our data showed that 31 brain metabolites could be detected in BLF, whereas only 21 metabolites could be recognized in CSF, suggesting that nearly 48% more metabolites could be found in BLF than in CSF. For those brain metabolites detected in both BLF and CSF, approximately 95% of them had higher concentrations in BLF than in CSF. Together, these data suggest that BLF might contain more potential biomarkers than CSF for the diagnosis of brain diseases. Accordingly, we identified BLF creatine as a potential diagnostic biomarker for glioma. In line with this, brain parenchymal creatine has been used in the clinical diagnosis of glioma, further supporting the potential promise of this diagnostic approach (19, 54, 55). Moreover, we identified DMA, DMG and glutamine as potential diagnostic biomarkers for viral infection and N-AG, O-AG,  $\alpha$ -glucose and AA as biomarkers for Parkinson's disease. While BLF has great potential for brain disease diagnosis, further minimally invasive surgery studies need to be performed to develop a strategy for the collection of BLF samples in human patients. The optimization of this strategy may require a long period of time, as many years have been needed to establish the surgery for CSF collection.

Together, the results our study systematically delineated the pathways of BLF drainage, and these findings may pave the way for the physiological study of the lymphatic system in the brain. We also developed a method to collect BLF and demonstrated that BLF has a better capacity than CSF to accurately reflect the pathophysiological status of the brain. Using this approach, we identified several potential diagnostic biomarkers for glioma, Parkinson's disease and

CNS infection. These findings may provide new insights into the diagnosis of CNS disorders.

## ACKNOWLEDGMENTS

This work was financially supported by the Fundamental Research Funds for the Central Universities [grant numbers: 2662017PY105, 510318177, 2662018PY025].

## CONFLICT OF INTEREST

The authors have declared that they have no conflict of interest.

## DATA AVAILABILITY STATEMENT

All data generated or analyzed during this study are included in this article.

## REFERENCES

- Alitalo K (2011) The lymphatic vasculature in disease. *Nat Med* **17**:1371–1380.
- Antila S, Karaman S, Nurmi H, Airavaara M, Voutilainen MH, Mathivet T et al (2017) Development and plasticity of meningeal lymphatic vessels. *J Exp Med* **214**:3645–3667.
- Aspelund A, Antila S, Proulx ST, Karlsten TV, Karaman S, Detmar M et al (2015) A dural lymphatic vascular system that drains brain interstitial fluid and macromolecules. *J Exp Med* **212**:991–999.
- Bakker EN, Bacskai BJ, Arbel-Ornath M, Aldea R, Bedussi B, Morris AW et al (2016) Lymphatic clearance of the brain: perivascular, paravascular and significance for neurodegenerative diseases. *Cell Mol Neurobiol* **36**:181–194.
- Bar-Klein G, Lublinsky S, Kamintsky L, Noyman I, Veksler R, Dalipaj H et al (2017) Imaging blood-brain barrier dysfunction as a biomarker for epileptogenesis. *Brain* **140**:1692–705.
- Beck C, Krutzmann A, Forkert ND, Juettler E, Singer OC, Köhrmann M et al (2014) A simple brain atrophy measure improves the prediction of malignant middle cerebral artery infarction by acute DWI lesion volume. *J Neurol* **261**:1097–1103.
- Begcevic I, Brinc D, Brown M, Martinez-Morillo E, Goldhardt O, Grimmer T et al (2018) Brain-related proteins as potential CSF biomarkers of Alzheimer's disease: a targeted mass spectrometry approach. *J Proteomics* **182**:12–20.
- Betterman KL, Harvey NL (2016) The lymphatic vasculature: development and role in shaping immunity. *Immunol Rev* **271**:276–292.
- Brinker T, Seifert V, Stolke D (1990) Acute changes in the dynamics of the cerebrospinal fluid system during experimental subarachnoid hemorrhage. *Neurosurgery* **27**:369–372.
- Carare RO, Hawkes CA, Jeffrey M, Kalaria RN, Weller RO (2013) Review: cerebral amyloid angiopathy, prion angiopathy, CADASIL and the spectrum of protein elimination failure angiopathies (PEFA) in neurodegenerative disease with a focus on therapy. *Neuropathol Appl Neurobiol* **39**:593–611.
- Card CM, Yu SS, Swartz MA (2014) Emerging roles of lymphatic endothelium in regulating adaptive immunity. *J Clin Invest* **124**:943–952.
- Chen J, He J, Ni R, Yang Q, Zhang Y, Luo L (2019) Cerebrovascular injuries induce lymphatic invasion into brain parenchyma to guide vascular regeneration in zebrafish. *Dev Cell* **49**:697–710.
- Da Mesquita S, Fu Z, Kipnis J (2018) The meningeal lymphatic system: a new player in neurophysiology. *Neuron* **100**:375–388.
- Dai H, Xiao C, Liu H, Hao F, Tang H (2010) Combined NMR and LC-DAD-MS analysis reveals comprehensive metabolomic variations for three phenotypic cultivars of *Salvia miltiorrhiza* Bunge. *J Proteome Res* **9**:1565–1578.
- Dai H, Xiao C, Liu H, Tang H (2010) Combined NMR and LC-MS analysis reveals the metabolomic changes in *Salvia miltiorrhiza* Bunge induced by water depletion. *J Proteome Res* **9**:1460–1475.
- Daneman R, Prat A (2015) The blood-brain barrier. *Cold Spring Harb Perspect Biol* **7**:a020412.
- Desai B, Hsu Y, Schneller B, Hobbs JG, Mehta AI, Linninger A (2016) Hydrocephalus: the role of cerebral aquaporin-4 channels and computational modeling considerations of cerebrospinal fluid. *Neurosurg Focus* **41**:E8.
- Duan Y, An Y, Li N, Liu B, Wang Y, Tang H (2013) Multiple univariate data analysis reveals the inulin effects on the high-fat-diet induced metabolic alterations in rat myocardium and testicles in the preobesity state. *J Proteome Res* **12**:3480–3495.
- Durmo F, Rydelius A, Cuellar Baena S, Askaner K, Lätt J, Bengzon J et al (2018) Multivoxel <sup>1</sup>H-MR spectroscopy biometrics for preoperative differentiation between brain tumors. *Tomography* **4**:172–181.
- van Etten ES, Verbeek MM, van der Grond J, Zielman R, van Rooden S, van Zwet EW et al (2017) beta-Amyloid in CSF: biomarker for preclinical cerebral amyloid angiopathy. *Neurology* **88**:169–176.
- Huang M, Dong XQ, Hu YY, Yu WH, Zhang ZY (2010) High S100B levels in cerebrospinal fluid and peripheral blood of patients with acute basal ganglial hemorrhage are associated with poor outcome. *World J Emerg Med* **1**:22–31.
- Iliff JJ, Wang M, Liao Y, Plogg BA, Peng W, Gundersen GA et al (2012) A paravascular pathway facilitates CSF flow through the brain parenchyma and the clearance of interstitial solutes, including amyloid beta. *Sci Transl Med* **4**:147ra111.
- Jessen NA, Munk ASF, Lundgaard I, Nedergaard M (2015) The glymphatic system: a beginner's guide. *Neurochem Res* **40**:2583–2599.
- Johanson CE, Duncan JA, Klinge PM, Brinker T, Stopa EG, Silverberg GD (2008) Multiplicity of cerebrospinal fluid functions: new challenges in health and disease. *Cerebrospinal Fluid Res* **5**:10.
- Johanson C, Johanson N (2016) Merging transport data for choroid plexus with blood-brain barrier to model CNS homeostasis and disease more effectively. *CNS Neurol Disord Drug Targets* **15**:1151–1180.
- Johanson C, Stopa E, Baird A, Sharma H (2011) Traumatic brain injury and recovery mechanisms: peptide

- modulation of periventricular neurogenic regions by the choroid plexus-CSF nexus. *J Neural Transm (Vienna)* **118**:115–133.
27. Johnston M, Zakharov A, Papaiconomou C, Salmasi G, Armstrong D (2004) Evidence of connections between cerebrospinal fluid and nasal lymphatic vessels in humans, non-human primates and other mammalian species. *Cerebrospinal Fluid Res* **1**:2.
  28. Kerjaschki D (2014) The lymphatic vasculature revisited. *J Clin Invest* **124**:874–877.
  29. Kida S, Pantazis A, Weller RO (1993) CSF drains directly from the subarachnoid space into nasal lymphatics in the rat. Anatomy, histology and immunological significance. *Neuropathol Appl Neurobiol* **19**:480–488.
  30. Koscova S, Zakova Slivarichova D, Tomeckova I, Melicherova K, Stelzer M, Janakova A *et al* (2017) Cerebrospinal fluid biomarkers in the diagnosis of Creutzfeldt-Jakob disease in Slovak patients: over 10-Year period review. *Mol Neurobiol* **54**:5919–5927.
  31. Kuo PH, Stuehm C, Squire S, Johnson K (2018) Meningeal lymphatic vessel flow runs countercurrent to venous flow in the superior sagittal sinus of the human brain. *Tomography* **4**:99–104.
  32. Laman JD, Weller RO (2013) Drainage of cells and soluble antigen from the CNS to regional lymph nodes. *J Neuroimmune Pharmacol* **8**:840–856.
  33. Lattanzio F, Abu-Rumeileh S, Franceschini A, Kai H, Amore G, Poggiolini I *et al* (2017) Prion-specific and surrogate CSF biomarkers in Creutzfeldt-Jakob disease: diagnostic accuracy in relation to molecular subtypes and analysis of neuropathological correlates of p-tau and A $\beta$ 42 levels. *Acta Neuropathol* **133**:559–578.
  34. Laubner S, Ondreka N, Failing K, Kramer M, Schmidt MJ (2015) Magnetic resonance imaging signs of high intraventricular pressure—comparison of findings in dogs with clinically relevant internal hydrocephalus and asymptomatic dogs with ventriculomegaly. *BMC Vet Res* **11**:181.
  35. Liao S, von der Weid PY (2015) Lymphatic system: an active pathway for immune protection. *Semin Cell Dev Biol* **38**:83–89.
  36. Lohrberg M, Wilting J (2016) The lymphatic vascular system of the mouse head. *Cell Tissue Res* **366**:667–677.
  37. Louveau A, Da MS, Kipnis J (2016) Lymphatics in neurological disorders: a neuro-lympho-vascular component of multiple sclerosis and Alzheimer's disease? *Neuron* **91**:957–973.
  38. Louveau A, Smirnov I, Keyes TJ, Eccles JD, Rouhani SJ, Peske JD *et al* (2015) Structural and functional features of central nervous system lymphatic vessels. *Nature* **523**:337–341.
  39. Lowhagen P, Johansson BB, Nordborg C (1994) The nasal route of cerebrospinal fluid drainage in man. A light-microscope study. *Neuropathol Appl Neurobiol* **20**:543–550.
  40. Minnerup J, Wersching H, Ringelstein EB, Heindel W, Niederstadt T, Schilling M *et al* (2011) Prediction of malignant middle cerebral artery infarction using computed tomography-based intracranial volume reserve measurements. *Stroke* **42**:3403–3409.
  41. Murtha LA, Yang Q, Parsons MW, Levi CR, Beard DJ, Spratt NJ, McLeod DD (2014) Cerebrospinal fluid is drained primarily via the spinal canal and olfactory route in young and aged spontaneously hypertensive rats. *Fluids Barriers CNS* **11**:12.
  42. Noé FM, Marchi N (2019) Central nervous system lymphatic unit, immunity, and epilepsy: is there a link? *Epilepsia Open* **4**:30–39.
  43. Paradot G, Baledent O, Gondry-Jouet C, Meyer ME, Le Gars D (2006) Cerebrospinal fluid flow imaging in the meningeal hemorrhage. *Neurochirurgie* **52**:323–329.
  44. Pirttila T, McHta PD, Soininen H, Kim KS, Heinonen O, Paljarvi L *et al* (1996) Cerebrospinal fluid concentrations of soluble amyloid beta-protein and apolipoprotein E in patients with Alzheimer's disease: correlations with amyloid load in the brain. *Arch Neurol* **53**:189–193.
  45. Preuss M, Hoffmann KT, Reiss-Zimmermann M, Hirsch W, Merckenschlager A, Meixensberger J, Dengl M (2013) Updated physiology and pathophysiology of CSF circulation—the pulsatile vector theory. *Childs Nerv Syst* **29**:1811–1825.
  46. Raper D, Louveau A, Kipnis J (2016) How do meningeal lymphatic vessels drain the CNS? *Trends Neurosci* **39**:581–586.
  47. Rasmussen MK, Mestre H, Nedergaard M (2018) The glymphatic pathway in neurological disorders. *Lancet Neurol* **17**:1016–1024.
  48. Ray B, Reyes PF, Lahiri DK (2011) Biochemical studies in Normal Pressure Hydrocephalus (NPH) patients: change in CSF levels of amyloid precursor protein (APP), amyloid-beta (A $\beta$ ) peptide and phospho-tau. *J Psychiatr Res* **45**:539–947.
  49. Schmid Daners M, Knobloch V, Soellinger M, Boesiger P, Seifert B, Guzzella L, Kurtcuoglu V (2012) Age-specific characteristics and coupling of cerebral arterial inflow and cerebrospinal fluid dynamics. *PLoS ONE* **7**:e37502.
  50. Schob S, Dieckow J, Fehrenbach M, Peukert N, Weiss A, Kluth D *et al* (2016) The cerebral surfactant system and its alteration in hydrocephalic conditions. *PLoS ONE* **11**:e0160680.
  51. Shapira Y, Artru AA, Lam AM (1992) Changes in the rate of formation and resistance to reabsorption of cerebrospinal fluid during deliberate hypotension induced with adenosine or hemorrhage. *Anesthesiology* **76**:432–439.
  52. Stoquart-ElSankari S, Balédent O, Gondry-Jouet C, Makki M, Godefroy O, Meyer ME (2007) Aging effects on cerebral blood and cerebrospinal fluid flows. *J Cereb Blood Flow Metab* **27**:1563–1572.
  53. Sun L, Tang Y, Yan K, Yu J, Zou Y, Xu W *et al* (2019) Differences in neurotropism and neurotoxicity among retrograde viral tracers. *Mol Neurodegener* **14**:8.
  54. Usinskiene J, Ulyte A, Bjørnerud A, Venius J, Katsaros VK, Rynkeviciene R *et al* (2016) Optimal differentiation of high- and low-grade glioma and metastasis: a meta-analysis of perfusion, diffusion, and spectroscopy metrics. *Neuroradiology* **58**:339–350.
  55. Wang Q, Zhang J, Xu W, Chen X, Zhang J, Xu B (2017) Role of magnetic resonance spectroscopy to differentiate high-grade gliomas from metastases. *Tumour Biol* **39**:1010428317110030.
  56. Weller RO, Djuanda E, Yow HY, Carare RO (2009) Lymphatic drainage of the brain and the pathophysiology of neurological disease. *Acta Neuropathol* **117**:1–14.
  57. Xiao C, Dai H, Liu H, Wang Y, Tang H (2008) Revealing the metabonomic variation of rosemary extracts using 1H NMR spectroscopy and multivariate data analysis. *J Agric Food Chem* **56**:10142–10153.
  58. Xie L, Kang H, Xu Q, Chen MJ, Liao Y, Thiyagarajan M *et al* (2013) Sleep drives metabolite clearance from the adult brain. *Science* **342**:373–377.



59. Zhong X, Wang J, Carlsson C, Okonkwo O, Zetterberg H, Li L (2019) A strategy for discovery and verification of candidate biomarkers in cerebrospinal fluid of preclinical Alzheimer's disease. *Front Mol Neurosci* **11**:483.
60. Zou W, Pu T, Feng W, Lu M, Zheng Y, Du R *et al* (2019) Blocking meningeal lymphatic drainage aggravates Parkinson's disease-like pathology in mice overexpressing mutated  $\alpha$ -synuclein. *Transl Neurodegener* **8**:7.

## SUPPORTING INFORMATION

Additional supporting information may be found in the online version of this article at the publisher's web site:

**Table S1.** The metabolites detected in the spectra of BLF and CSF with assessments achieved using a series of 2D NMR spectra.